Monthly Notices of the ROYAL ASTRONOMICAL SOCIETY
MNRAS **0,** L1–L0 (2023) https://doi.org/10.1093/mnrasl/slad106

Contextual characterization study of Chandrayaan-3 primary landing site

K. Durga Prasad,[1] Megha Bhatt ,[1] Amitabh,[2] G. Ambily,[1,3] Sachana Sathyan,[1,4] Dibyendu Misra,[1,5] Neeraj Srivastava[1] and Anil Bhardwaj [1]

[1]*Physical Research Laboratory, Ahmedabad 380009, India*
[2]*Space Applications Centre (ISRO), Ahmedabad 380015, India*
[3]*Department of Engineering Physics, Andhra University, Visakhapatnam-530003, India*
[4]*Department of Geology, University of Kerala, Trivandrum 695581, India*
[5]*Indian Institute of Technology Gandhinagar, Gandhinagar 382055, India*

Accepted 2023 July 27. Received 2023 July 27; in original form 2023 July 12

ABSTRACT

Chandrayaan-3 is an upcoming lunar mission of India aimed at soft landing and carrying out first-ever *in situ* investigations at a high-latitude location on the Moon. Chandrayaan-3 consists of a propulsion module, a lander and a rover, that carry a set of payloads for conducting *in situ* science experiments. In this work, contextual characterization of the primary landing site (PLS) located at 69.367621˚S, 32.348126 ˚E is carried out in terms of identification, geomorphology, composition, and thermophysical context using the best-ever high-resolution data sets. Our geomorphological study indicates that the PLS is safe for landing with slope less than 4˚ in about 78 per cent of landing area and an average elevation variation of about 169 m. The spectral analysis suggests that the region must have experienced extensive space weathering. Compositional analysis indicates that the landing region has a typical highland type of soil characteristics with Mg (4.3–5.2 wt. per cent), Fe (4.2–4.9 wt. per cent), Ca (10–11 wt. per cent), and Ti (0.25–0.35 wt. per cent). Thermophysical analyses show ∼30 and 175 K variability in spatial and diurnal temperatures at the PLS – an indicative of a local terrain of distinctive thermophysical characteristics. With important science instruments onboard, Chandrayaan-3 will provide a unique opportunity towards looking at localized variations leading to an improved understanding of the lunar surface.

Key words: methods: data analysis – methods: observational – methods: numerical – techniques: spectroscopic – Moon – planets and satellites: composition – planets and satellites: surfaces.

1. INTRODUCTION

The past decade has witnessed a dawn of renewed interest in lunar exploration, due to its scientific importance, with missions such as Chandrayaan-1, SELENE, Lunar Reconnaissance Orbiter (LRO/LCROSS), Chang'E 1–Chang'E 5 (Ohtake et al. 2008; Goswami et al. 2009; Vondrak et al. 2010; Ouyang et al., 2010; Colaprete et al. 2012). Continued to these, various space agencies, including the private ones, have flown and planning to fly several landing and roving missions to the Moon to test new technologies of landing and roving and for achieving specific scientific goals (Goswami and Annadurai 2011; Zuber et al. 2013; Angelopoulos 2014; Zuo et al. 2014; Horanyi et al. 2015; Li et al. 2015; Ju et al. 2017; Jia et al. 2018; Crusan et al. 2019; Gibney 2019; Hardgrove et al. 2019; Shyldkrot et al. 2019; Cohen et al. 2020; Dandouras et al. 2020; Gardner et al. 2021; Mitrofanov et al. 2021; Xiao et al. 2021). Recently, NASA with its ARTEMIS and Commercial Lunar Payload Services programmes, has comeback with its attempts for establishing a sustainable human presence on the Moon (Angelopoulos 2014; Creech et al. 2022). India also continues the legacy of its first Moon mission, Chandrayaan-1, with its follow-up orbiter Chandrayaan-2 (Goswami and Annadurai 2011). Chandrayaan-3 is an upcoming lunar mission of India consisting of an indigenous lander module with a rover and a propulsion module (Bhardwaj 2021). It is expected to be launched by mid-July 2023. The key objective of this mission is to demonstrate the soft-landing capability at a high-latitude region, roving in the vicinity and conducting a set of *in situ* experiments (https://www.isro.gov.in/Chandrayaan3_New.html). There are seven scientific payloads onboard, in which four are on the lander, two on the rover, and one on the propulsion module. The lander payloads, RAMBHA-LP (Radio Anatomy of Moon Bound Hypersensitive Ionosphere and Atmosphere – Langmuir Probe; Manju 2020), ChaSTE (Chandra's Surface Thermophysical Experiment; Durga Prasad et al. 2016), and ILSA (Instrument for Lunar Seismic Activity; John et al. 2020) will be analysing lunar atmosphere, surface thermophysical properties, and near-surface seismic activity, respectively. NASA's passive Laser Retroreflector Array is also accommodated on the lander for lunar laser ranging studies (Currie et al. 2011). The two rover payloads, Alpha particle X-ray spectrometer (APXS; Shanmugam et al. 2020) and laser induced breakdown spectrometer (LIBS; Laxmiprasad et al. 2013) are aimed at determining the elemental composition of lunar soil in the vicinity of the landing site. In addition to these, the propulsion module carries SHAPE (https://www.isro.gov.in/chandrayaan3_science.html) payload to study the polarimetric signatures of Earth from the Moon.

⋆ E-mail: durgaprasad@prl.res.in

Appropriate landing site selection and characterization is one of the most important aspects for successful soft landing and science exploration of Chandrayaan-3 mission. Selection of a landing site for Chandrayaan-3 was based on both technical (safe landing, local mobility, and operational constraints) and scientific (surface composition, local geology, and thermophysical environment) criteria. These criteria are in turn governed by various factors such as regional and local topography for safe landing and mobility, illumination, and temperature for operation, composition, geology, and local environment for science. Therefore, the mission needs to be supported by a well-defined context, both for landing feasibility and scientific exploration. Based on these considerations, eight sites were initially considered for feasibility study, out of which two sites (primary and alternate/backup) have been finally identified for Chandaryaan-3 landing and exploration (Fig. 1). The primary landing site (PLS) is proposed to be at 69.367621°S, 32.348126 E (https://www.isro.gov.in/Chandrayaan3_New.html), which is around 42 km away from the earlier planned Chandrayaan-2 landing site. This site lies between Manzius U and Boguslawsky M craters. Additionally, an alternate or a backup landing site, ∼450 km west to PLS, is also proposed, which is at 69.497764°S, 17.330409°W (Personal communication). Both are highland regions, with relatively flat surfaces. The landing area is constrained to ∼4 km × 2.4 km area centred at the site coordinates. Detailed contextual analyses of the proposed landing sites are necessary, both for planning mission operations and interpretation of science data obtained from onboard instruments. Understanding the local terrain, slopes, illumination, and surface temperatures is important for safe landing, carry out lander operations, and dictating the mobility path of the rover. On the other hand, geological, geomorphological, and thermophysical characterization a priori becomes significant for planning science operations, data interpretation, and finally deriving optimum science from the instruments onboard. With this in aim, we have carried out a contextual characterization study of the proposed PLS of Chandrayaan-3 mission within the landing area of ∼4 km × 2.4 km using all relevant data sets available. We have also used Chandrayaan-3 specific targeted observations from Chandrayan-2 orbiter, particularly the best spatial resolution (25 cm) images from Orbiter High Resolution Camera (OHRC; Chowdhury et al. 2019) and derived digital elevation model (DEM) for this study.

2. DATA SETS AND MODEL USED IN THIS STUDY

Multiple data sets from Chandrayaan-1, Chandrayaan-2, SELENE, and LRO missions have been used for studying the Chandrayaan-3 landing site. These include data sets from (a) high-resolution ortho images and derived DEM from OHRC onboard Chandrayaan-2. OHRC is capable of providing images at a spatial resolution of ∼25 cm with 3 km of swath at two view angles (∼5° and 25°) in two consecutive orbits by spacecraft manoeuvring (Choudhary et al. 2019; Amitabh et al. 2021). These images were used to generate a high-resolution DEM in OPTIMUS (OPTIMal UndulationS) software. All the images were analysed using ARCGIS and QGIS software and projected in the equirectangular coordinate system. (b) Spectral data acquired by the Moon Mineralogy Mapper (M^3) in optical period 2C (∼280 m pixel^{-1}; 85 spectral bands, and 0.46–3.00 μm wavelength range) of Chandrayaan-1 (Pieters et al. 2009). (c) Topography data from LRO LOLA (Lunar Orbiter Laser Altimeter; Smith et al. 2010) co-registered with SELENE, NAC, and WAC. (d) Surface temperature data sets from Diviner radiometer onboard LRO (Paige et al. 2010). We have also used a three-dimensional thermophysical model to understand the local thermophysical behaviour of the landing site (Durga Prasad et al. 2022). Details of these data sets, model, and their processing methodology is given in their respective sections.

3. LANDING SITE CHARACTERIZATION AND HAZARD IDENTIFICATION

The Chandrayaan-3 landing site selection (Fig. 1) is based on a high-latitude location with slopes less than 10°, boulders less than 0.32 m of diameter, continuously sunlit for at least 11–12 d, clear radio visibility, less craters, and boulders and with topography of local terrain that do not cast shadows for long durations. The Chandrayaan-3 primary and ALSs (Fig. 1b) are finalized after a systematic search from 20 candidate sites within the 60°S to 70°S latitudes (Amitabh et al. 2023). Out of these 20 candidate sites, 8 sites satisfied the required criteria and were further studied in detail using the best spatial resolution OHRC images (Fig. 1a) The main characteristics of all the eight shortlisted sites are given in supplementary Table 1. The OHRC images were also used for deriving the best spatial resolution DEM of the landing site at 0.32 m grid interval with a height resolution of 0.05 m (Choudhary et al. 2019; Amitabh et al. 2021). Based on OHRC DEMs and ortho images the terrain undulations, slope, aspect, and illumination conditions were studied in order to narrow down at three sites. For all the three sites, one additional criteria of distribution of safe grids of 24 m × 24 m, 36 m × 36 m, and 48 m × 48 m inside the selected landing area of ∼4 km × 2.4 km were considered. Based on this additional condition, PLSs and ALSs were selected. The PLS is finalized based on better safe grid distribution in the entire area of 4 km × 2.4 km. Additionally, it provides flexibility for the lander to land at any place within a distance of 100 m from the lander hovering point. OHRC derived map of hazards based on illumination and safe grids is given in Fig. 2.

4. RESULTS AND DISCUSSION

In line with the primary objective of this study, we have carried out a detailed geomorphological, spectroscopic, and thermophysical analyses of the landing site using all possible data sets available. Details of these analyses and results obtained and inferences therein are discussed in the following sections.

4.1. Chandrayaan-3 PLS: geomorphology

Fig. 3 shows a set of maps depicting geomorphology of the PLS. All maps have been derived from OHRC ortho and stereo images (https://www.issdc.gov.in/isda.html). We found that the PLS area is smooth, flat, and high in albedo. This region comes under light plains as per the global light plain map derived from LRO (Meyer et al. 2020). We examined the slope and roughness of the PLS using OHRC to understand the geomorphology. The maximum slope of a point is determined using the distance and elevation difference between two adjacent grid cells of DEM data, and the square root of the sum of their squares as described in Wu et al. (2014). This was achieved using spatial analyst tool of ARCGIS software. We set our minimum criteria satisfied by the terrain as it should be flat with minimum slope (<7°) and roughness (<0.4), similar to Chandrayaan-2 landing site (Sinha et al. 2020). The geomorphology of extended region around Chandrayaan-3 landing site is given in Sinha et al. (2023). Here, we have restricted our analysis to only the landing area for understanding localized variations. The elevation profile, slope,

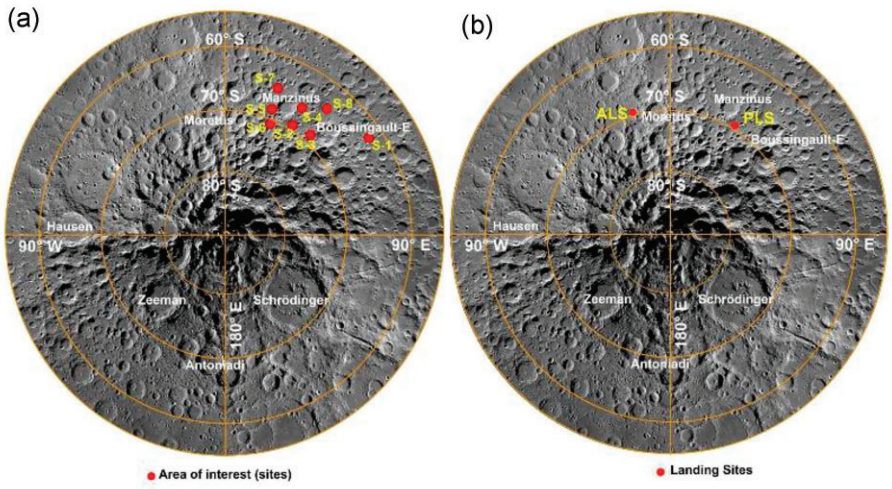

Figure 1 (a) Locations of landing sites (S-1 to S-8) considered for Chandrayaan-3 using OHRC Images. (b) Selected sites – PLS and alternate landing site (ALS). Images used are taken from WAC of LRO.

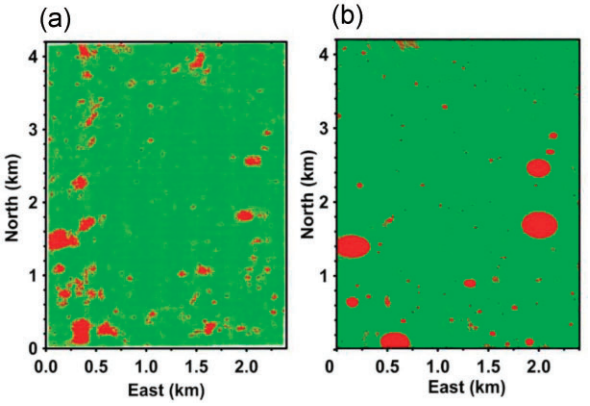

Figure 2. OHRC derived hazard maps. (a) Illumination map in terms of sunlit for minimum 11 d (red-shadow, green-illuminated). (b) Distribution of safe grid for landing within 48 m × 48 m (green-safe, red-hazard).

and roughness of the PLS were generated from the DEM. Minimum elevation variation with the ground distance is shown from the four different elevation profile sections, made across the centre of the landing area of 4.5 km × 2.5 km (see Figs 3(b) and 3(e) showing that the average elevation variation is about 169 m within the landing area). We calculated roughness as the deviation from a mean plane which is a plane that best fits the terrain by taking the ratio of differences: 'mean height–minimum height' to 'maximum height–minimum height'. It was observed that most highly elevated regions are situated toward the west of the landing area and the elevation gradually decreases moving towards the east. As shown in Fig. 3(e), a variation in this general trend can be observed for the profile C–C' where the landing point is located in a 25–45 m less elevated area compared to SE–NW parts also shown in Fig. 3(c) in terms of colour-coded DEM. Around 78 per cent of the area has a slope of less than 4° and higher slopes areas are very limited which might be hazardous for rover operation. Relatively higher slopes were found only in crater walls and ejecta layers.

Geomorphologically, the terrain is old and belongs to the Nectarian terra plain unit (Wilhelms et al. 1979; Fortezzo et al. 2020) dominantly covered by ejecta layers from secondary craters of Manzinus and Boguslawsky craters. The western region is covered by ejecta deposits exhibiting random slope breaks, which can be attributed due to the ejecta from secondary crater of Manzinus while the eastern region comprises ejecta deposits from the secondary craters of Manzinus and Boguslawsky with gentle slope breaks. The central region is comparatively smooth and very gently sloping towards all directions demonstrating that PLS is a perfect spot for landing. A map of geomorphic units and some crater types in the landing region are shown in Fig. 4. As shown in Fig. 5, several fresh craters (green) and boulders (blue) were identified within the landing area that can be potential sampling locations for the rover and can assist in planning the rover mobility.

4.2. Spectral analysis and elemental abundances of Chandrayaan-3 landing site

We used the M^3 hyperspectral level 2 reflectance data (Pieters et al. 2009) for understanding the mineralogy and chemical composition of the PLS. Two M^3 hyperspectral data sets obtained from optical period 2C (Green et al. 2011) covered the Chandrayaan-3 PLS.

The data sets are downloaded from the planetary data system (PDS) node of the Jet Propulsion Laboratory (https://pds-imaging.jpl.nasa.gov/volumes/m3.html). The M^3 level 2 reflectance data is thermally and photometrically calibrated. Statistical polishing and band mask is applied to reduce the noise and artefacts (Pieters et al. 2009; Boardman et al. 2011; Green et al. 2011). The M^3 data are also used for estimating the average abundances of Fe, Ti, Mg, and Ca of PLS using the global elemental abundance maps at 1.5 km pixel^{-1} spatial resolution (Bhatt et al. 2019). The M^3 IDs, M3G20090606T093322 and M3G20090606T010302 of OP2C covered the Chandrayaan-3 PLS for which generally the SNR is poor at high latitudes. We used both data sets for the spectral analysis of PLS to avoid misinterpretation. Fig. 6 shows a 1° × 1° albedo image of the M^3, about 250 M^3 footprints/per M^3 image belong within the PLS-defined landing area.

The M^3-based spectral analysis suggests that the PLS region is majorly highland-type soil with no prominent absorption features at 1000 and 2000 nm. A few craters on the western side show a weak absorption feature around 900 nm. Due to poor SNR for OP2C M^3 data mainly at high latitudes, we could not identify any

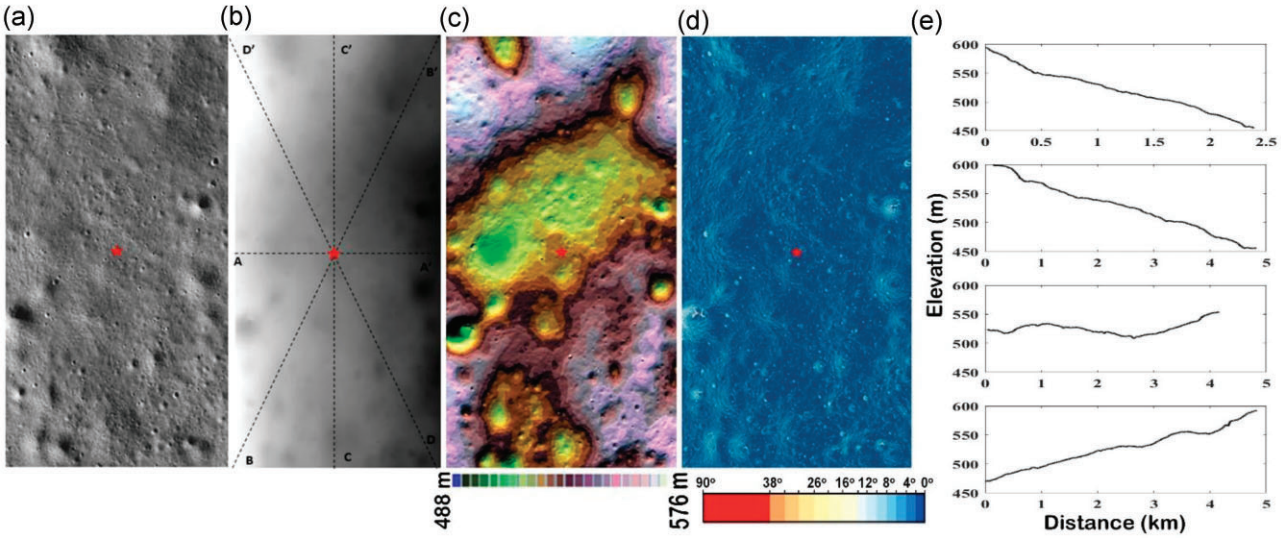

Figure 3 Detailed geomorphologic maps of the landing region (a) OHRC ortho image. (b) OHRC derived DEM. (c) Colour coded DEM. (d) Slope map. (e) Elevation profiles through A–A', B–B', C–C', and D–D'.

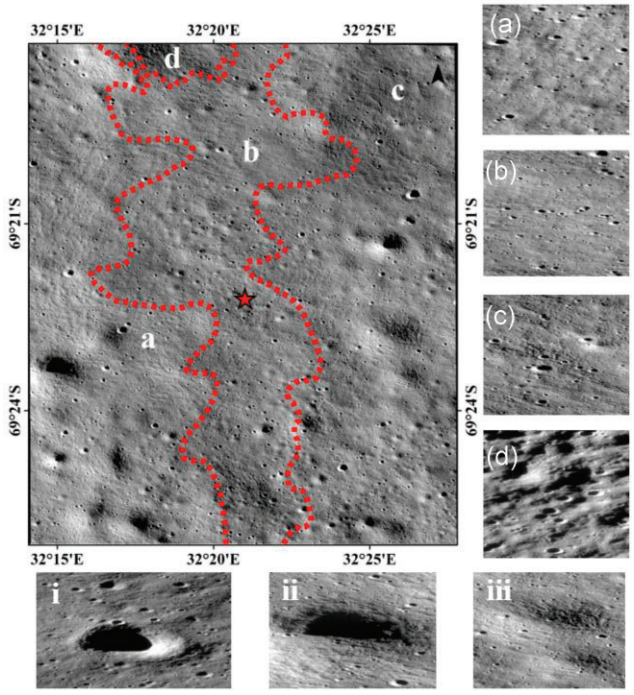

Figure 4 Geomorphic units of the landing area. (a–d) The entire area was divided into three units. The unit 'a' was mainly formed by the ejecta of secondary craters of Manzinus with more pronounced slope breaks whereas the unit 'c' was the comparatively wider ejecta layer formed by secondary craters. Unit 'd' was formed by the ejecta layer deposition from the Manzinus U crater located at north of the landing site. In between units 'a', 'c', and 'd', there is unit 'b' that has a nearly flat terrain with gently sloping. (i–iii) Three different crater types were mentioned around the PLS of Chandrayaan-3. (i) Fresh crater of 85 m diameter from west of landing point having some boulders in its western rim. (ii) A 300 m diameter degraded crater. (iii) Ghost craters are located at the east of the landing site.

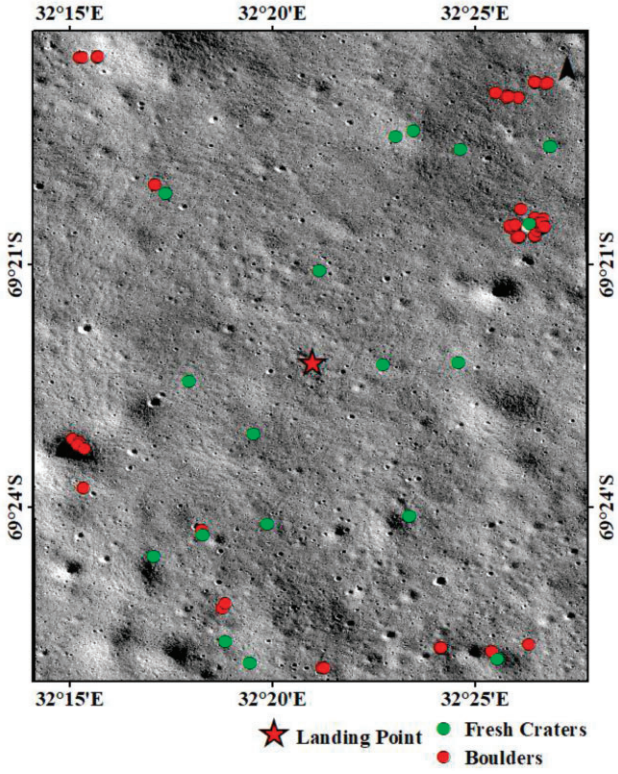

Figure 5 Potential sampling sites in the form of fresh craters (green) and boulders (red) were observed around the probable PLS (red star) of Chandrayaan-3.

spectral signature with the presence of an absorption band around 2000 nm. The PLS belongs to Nectarian plains (Wilhelms et al. 1979) indicating that the region must have experienced extensive space weathering and crater ejecta of several craters and South Pole Aitken basin must have deposited on this site. The space weathering affects a spectral signature by reducing the mineral absorption band depth and albedo, and by increasing the spectral continuum slope (Fischer

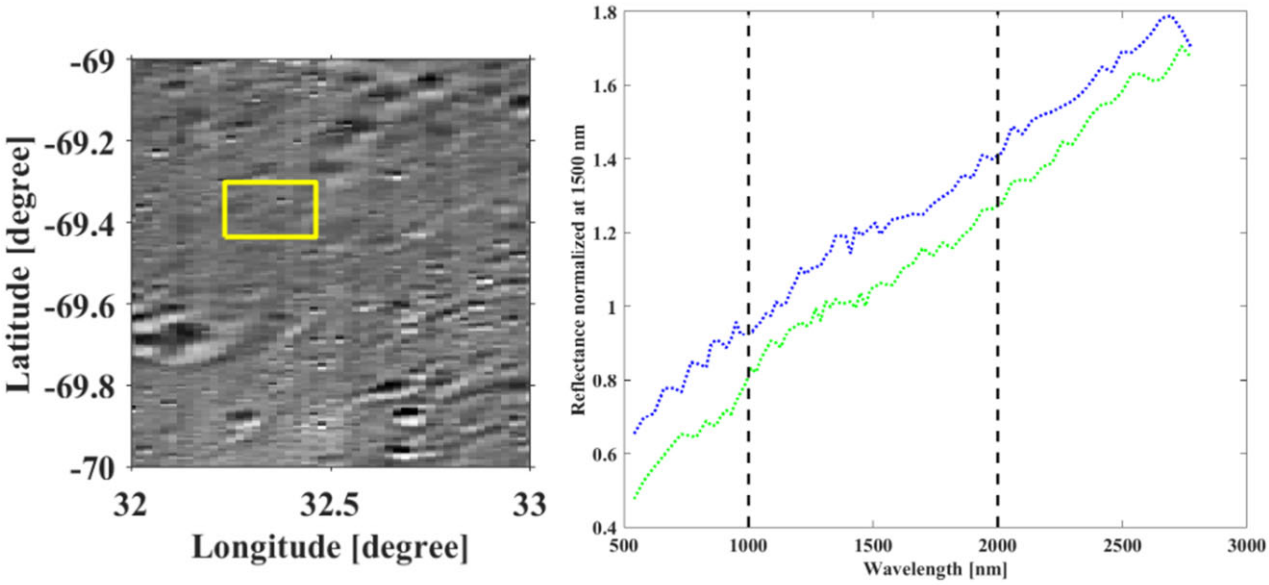

Figure 6 (a) $1^o \times 1^o$ M^3 albedo image covering Chandrayaan-3 PLS region at ∼1500 nm. The PLS region is marked as a yellow square. (b) Extracted normalized representative spectra from PLS (yellow box). The most common spectral signature is represented in blue colour without having any significant absorption feature at 1000 and 2000 nm. The spectra represent highland-type soil. A few fresh and small craters show a weak absorption band around 900 nm and are shown here in green colour. For clarity, an offset of 0.02 is applied to the spectrum in green colour. The hydroxyl/H_2O spectral signature around 2800 nm is present in both the representative spectra.

and Pieters, 1996; Hapke 2001; Pieters and Noble 2016). The weak mineralogical spectral signature gets masked due to the presence of space weathering and the absorption band around 2000 nm is mainly affected due to an increase in reddening. The Chandrayaan-3 PLS spectral trends are comparable to Chandrayaan-2 PLS spectral trends (Sinha et al. 2020). We also examined the average elemental abundances of the Chandrayaan-3 PLS using global maps of Fe, Mg, Ca, and Ti (Bhatt et al. 2015, 2019). Mg varies in the range of 4.3–5.2 wt. per cent, Fe varies from 4.2 to 4.9 wt. per cent, Ca is in the range of 10–11 wt. per cent, and Ti is very low within the range of 0.25–0.35 wt. per cent. The spectral analysis and average elemental abundance of the Chandrayaan-3 PLS suggest that the region is covered by the highland type of composition.

4.4. Temperatures and thermophysical characterization

Understanding the landing site characteristics in thermal and thermophysical perspective is another important aspect that drives both the mission operations and science. Therefore, we have carried out a detailed thermophysical characterization of the landing site at both regional and local scales. An idea of the peak temperature and its variability in the vicinity of the landing site is an important parameter that dictate the operations, survivability, and lifetime of both the lander and rover. On the other hand, a priori understanding of the thermophysical characteristics of the surface and subsurface will be also be helpful in the interpreting the data obtained from ChaSTE instrument and constructing the geophysical perspective of the landing site using another onboard instrument, ILSA.

Therefore, temperatures and thermophysical characteristics of the landing site were analysed using all possible available data sets and 3D modelling. Digital elevation data from LOLA and OHRC is used to understand the terrain at both regional and local scales. Data for surface temperatures and thermophysical parameters covering the landing area was used from DIVINER observations. Using these

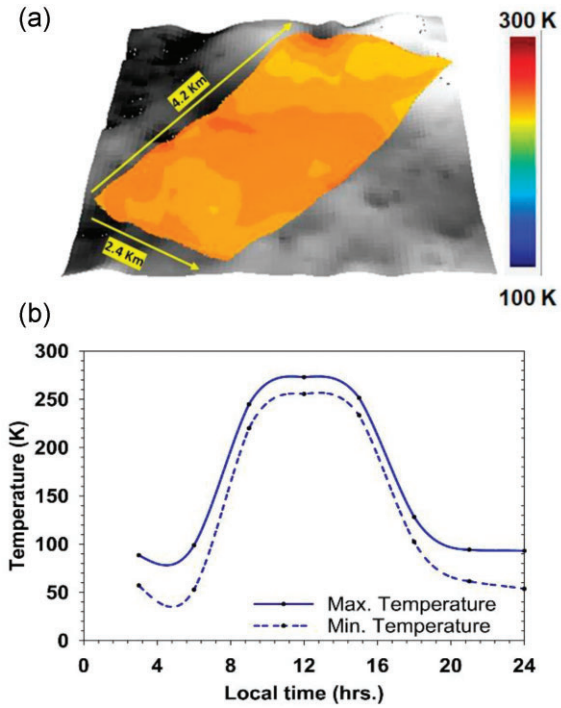

Figure 7 (a) Local surface temperature variations for the landing area at local noon. (b) Diurnal variation of minimum and maximum temperatures at the landing site.

data sets and methodology described in supplementary material, 3D temperature maps for each local time were generated for the landing site. Fig. 7(a) shows the spatial variability of local surface temperatures within the landing area corresponding to local noon. While, surface temperature maps were derived for different local

Table 1. Table showing minimum and maximum temperatures from LRO DIVINER at different phases of the day in both local and regional perspectives for the PLS.

Local time (h)	CH3-PLS – 4 km × 2.4 km		CH3-PLS – 25 km × 25 km	
	Max T (K)	Min T (K)	Max T (K)	Min T (K)
Dawn (6.00)	98.65	52.78	141.78	53.47
Noon (12.00)	273.02	244.53	300.06	200.70
Dusk (18.00)	128.18	96.05	144.00	73.57
Midnight (24.00)	93.00	53.63	98.96	49.69

times corresponding to various phases of the lunar day (midnight, dawn, noon, and dusk), temperature plot corresponding to local noon is shown in Fig. 7(a) as maximum temperature variability is expected only during that time. As the landing area is relatively small (~4 km × 2.4 km), spatial variability of surface temperatures within it is not expected. In contrast, a significant spatial variability of ~30 K is seen as illustrated in Fig. 7(a). It is important to note that this spatial variation of ~30 K corresponds to temperature data at a resolution of ~250 m pixel^{-1}, the best resolution possible from Diviner. This implies that further spatial contrast in temperatures may be expected at a highly localized scale of few 10s of metres. The diurnal variations of maximum and minimum surface temperatures were also derived for the landing site and shown in Fig. 7(b). The diurnal variation is as expected and reported in earlier literature (Vasavada et al. 1999; Hayne et al. 2017; Durga Prasad et al. 2022). As seen in Fig. 7(b), a maximum variation of ~175 K is reported within the landing region. Being a high-latitude (60–70°) site, the diurnal temperatures have seen to be varying between 310 and 340 K. For comparison, surface temperatures for regional scale area of ~25 km × 25 km were also analysed. The surface temperatures obtained at various local times for both local and regional areas of the landing site are given in Table 1. It can be seen that the variation between the maximum and minimum temperatures were found to be very less for 4 km × 2.4 km area, when compared to the 25 km × 25 km area. One reason could the less data coverage from Diviner in those areas. Else, it can also be attributed to the distinct thermophysical behaviour at regional and local scales as reported by some earlier workers. In any case, it is an interesting aspect to understand. Data from ChaSTE experiment onboard Chandrayaan-3 lander are expected to provide some explanation for these observations.

4.3.1. Regolith thickness and influence on local thermophysical behaviour

The H-parameter for PLS is also analysed and shown in supplementary figure 1. H-parameter gives the average thickness of the uppermost fluff layer, thus providing the thermal inertia of the given site. More the value of H-parameter, thicker the surficial insulating material would be (Hayne et al. 2017). It is interesting to note that the thermal inertia exhibits significant variations around the PLS landing ellipse. The H-parameter for the PLS 4 km × 2.4 km site is seen to be varying between 0.06 and 0.09 m, which should largely affect the thermophysical behaviour of the surface. Thus, the proposed landing at any given point will influence the thermophysical measurements and is expected to be greatly different from the surrounding areas.

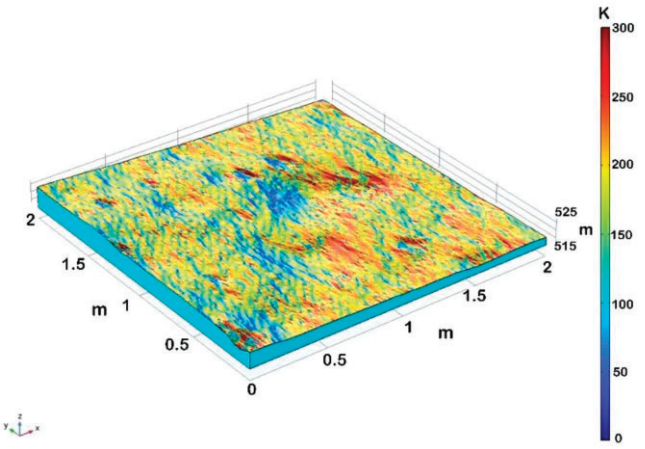

Figure 8 Model derived surface temperature variation within 200 m × 200 m area at the centre of the landing site, during dawn phase, depicting distinct thermophysical behaviour at local scale.

4.3.2. Expected local scale thermophysical behaviour

Since the landing site is located at high latitude and exhibits a significant variation in surface temperatures as seen from Diviner data, understanding the near-surface thermophysical behaviour also becomes crucial in mission perspective. Therefore, a three-dimensional thermophysical model study is carried out for the landing site (Durga Prasad et al. 2022). The model can simulate the lunar surface as a multilayered system with specific thermophysical parameters. A local scale (few metres) study is carried out for the PLS. For this study, the parameters such as thermal conductivity, and specific heat are described as analytic functions, and boundaries are given thermally insulated. The surface is generated from the high-resolution OHRC DEM from Chandrayaan-2. This data is used in order to import even a small topographic variation at the landing site. A 200 m × 200 m area, centred at the centre coordinates of the landing site is selected. The thickness of the fluff is taken to be 9 cm, which is resonant with the H-parameter map (Hayne et al. 2017). The entire geometry is meshed into finer elements, with element sizes varying between 0.8 m to 11m. Model simulations were carried out using appropriate parameters and conditions described in Durga Prasad et al. (2022). Fig. 8 gives the model derived surface temperatures for a small area of 200 m × 200 m around the centre of the landing area during local dawn phase. Distinct temperature variations at local scales of few metres are clearly seen within the small area. Such a variation could be either due to distinct physical characteristics of the locations or due to local topographic variation. More explanation can be provided by *in situ* observations from Chandrayaan-3.

5. CONCLUSION

In this letter, we presented the detailed contextual investigation of the PLS of Chandrayaan-3 mission in terms of landing site identification, geomorphological, compositional, and thermophysical context. Using the best-ever high resolution OHRC DEMs and ortho images, PLS has been fully characterized with respect to terrain undulations, slope, aspect, and illumination. Our geomorphological study based on the best spatial resolution data of recent times from OHRC indicate that the PLS is safe for landing and for rover operation. The rover will be following the exploration path mainly based on the sun movement from east to west and will encounter mainly morphology formed by the ejecta of secondaries. It will be interesting to examine

vicinity of fresh craters to develop local stratigraphy based on the crater diameter to excavated depth ratio. The spectral analysis of PLS region in visible–near-infrared wavelength region suggest that the region must have experienced extensive space weathering and represent typical highland type of soil characteristics. The outcomes of our spectral study will be a guiding point for APXS and LIBS onboard Chandrayaan-3 rover which will be mainly looking to local scale compositional and mineralogical differences. The PLS is dominated by secondary craters of metre scale diameter which are mainly responsible for regolith churning and do not excavate materials from deeper crust/mantle. However, as the lunar regolith formation and evolution is a complex process in which the smaller craters remix and redistribute the already existing regolith layer, it will be interesting to map local scale compositional variations using APXS. The effect of solar and cosmic particles dominates the regolith upper layer and increase with increase in maturity of the surface. However, APXS is insensitive to space weathering induced variations and mainly providing insights on compositional differences due to churning of regolith at local scale. A detailed thermophysical analysis of PLS revealed a significant diurnal and spatial variability of surface temperatures. This directs towards a local terrain of distinctive thermophysical characteristics within the landing region. Thus, the proposed landing at any given point will influence the thermophysical measurements and is expected to be greatly different from the surrounding areas. Significant variation of thermal inertia or the thickness of the outermost layer as seen around the PLS landing area could largely affect the thermophysical behaviour of the surface and subsurface. It is necessary for understanding the stability of regolith bound water–ice at the surface/shallow subsurface – an important aspect for future lunar *in situ* resource utilization studies. *In situ* data from ChaSTE experiment will be able to provide validation and further understanding towards this. With important science instruments onboard and being the first-ever high-latitude measurement, Chandrayaan-3 is definitely going to open up new vistas in the understanding of lunar science.

ACKNOWLEDGEMENTS

We thank the Department of Space, Government of India for providing the financial support for carrying out this work. AB was supported by J. C. Bose Fellowship during the period of this work. We thank Shri Nilesh M. Desai – Director, Space Applications Centre (SAC), Ahmedabad and Shri Debajyoti Dhar – DD, SIPA, SAC, Ahmedabad, for providing necessary support for carrying out data analysis of OHRC. We thank Chandrayaan-3 mission project teams and ISSDC for their data support. We thank Department of Science and Technology (DST), Government of India, for supporting G. Ambily & Sachana Sathyan under INSPIRE Fellowship. The local scale model computations were performed on the PARAM Vikram-1000 High Performance Computing Cluster of the Physical Research Laboratory, Ahmedabad. Reviewer's suggestions are thankfully acknowledged.

DATA AVAILABILITY

The data used in this work will be available upon request

REFERENCES

Amitabh et al. 2021, In 52nd Lunar and Planetary Science Conference, held 15-19 March, 2021 at The Woodlands, Texas and virtually. LPI Contribution No. 2548, High Resolution DEM Generation from Chandrayaan-2 Orbiter High Resolution Camera Images. p. 1396

Amitabh, Suresh K., Prashar A. K., Suhail. 2023, In 54th Lunar and Planetary Science Conference, held 13-17 March, 2023 at The Woodlands, Texas and virtually. LPI Contribution No. 2806, id.1037, Terrain Characterisation of Potential Landing Sites for Chandrayaan-3 Lander using Orbiter High Resolution Camera (OHRC) Images

Angelopoulos V., 2014, The ARTEMIS Mission. p. 3

Bhardwaj A., 2021, In 43rd COSPAR Scientific Assembly during Jan. 28 - Feb. 4,in Sydney, Australia (virtually), Vol. 43, p. 765, published by COSPAR

Bhatt M., Mall U., Woehler C., Grumpe A., Bugiolacchi R., 2015, Icarus, 248, 72

Bhatt M., Wöhler C., Grumpe A., Hasebe N., Naito M., 2019, A&A, 627, 155

Boardman J. W. et al. 2011, J. Geophys Res. Planets, 116, E00G16

Chowdhury A. R. et al. 2019, Curr. Sci., 117, 560

Cohen B. A., Hayne P. O., Greenhagen B., Paige D. A., Seybold C., Baker J., 2020, IEEE Aerosp. Electron. Syst. Mag., 35, 46

Colaprete A., Elphic R. C., Heldmann J., Ennico K., 2012, Space Sci. Rev., 167, 3

Creech S., Guidi J., Elburn D., 2022, IEEE Aerospace Conference (AERO), IEEE, New York, p. 1

Crusan J., Galica C., 2019, Acta Astronaut., 157, 51

Currie D., Dell'Agnello S., Delle Monache G., 2011, Acta Astronaut., 68, 667

Dandouras I. et al. 2020, Space Sci. Rev., 216, 1

Durga Prasad K., 2016, Annual Report 2015 16-00, Front-End Electronics Development for ChaSTE Payload onboard Chandrayaan-2 Lander. Physical Research Laboratory, Navrangpura, Ahmedabad

Durga Prasad K., Rai V. K., Murty S. V. S., 2022, Earth Space Sci., 9, 12

Fischer E. M., Pieters C. M., 1996, J. Geophys Res. Planets, 101, 2225

Fortezzo C. M., Spudis P. D., Harrel S. L., 2020, In 52nd Lunar and Planetary Science Conference, held 15-19 March, 2021 at The Woodlands, Texas and virtually. LPI Contribution No. 2326

Gardner T., Cheetham B., Forsman A., Meek C., Kayser E., Parker J., Thompson M., 2021, Capstone: A cubesat pathfinder for the lunar gateway ecosystem

Gibney E., 2019, Nature, 566, 434

Goswami J. N., Annadurai M., 2009, Curr. Sci., 486

Goswami J. N., Annadurai M., 2011, In 42nd Lunar and Planetary Science Conference, held 7-11 March, 2011 at The Woodlands, Texas and virtually. LPI Contribution No. 2042

Green R. O. et al. 2011, J. Geophys Res. Planets, 116, E00G19

Hapke B., 2001, J. Geophys Res. Planets, 106, 10039

Hardgrove C., Starr, R., Lazbin, I., Babuscia, A., Roebuck, B., DuBois, J., Struebel, N., Colaprete, A., Drake, D., Johnson, E. and Christian, J. 2020 2020. The lunar polar hydrogen mapper CubeSat mission. IEEE Aerospace and Electronic Systems Magazine, 35(3), pp.54-69.

Hayne P. O. et al. 2017, J. Geophys Res. Planets, 122, 2371

Horanyi M. et al. 2015, in Elphic R., Russell C., eds, The Lunar Atmosphere and Dust Environment Explorer Mission (LADEE), Springer, Berlin, p. 93, https://www.isro.gov.in/Chandrayaan3_New.html

Jia Y., Zou Y., Ping J., Xue C., Yan J., Ning Y., 2018, Planet. Space Sci., 162, 207

John J. et al. 2020, Curr. Sci., 118, 376

Ju G., 2017, Korean pathfinder lunar orbiter (KPLO) status update. In Annual Meeting of the Lunar Exploration Analysis Group (LEAG) Conference, Columbia, MD. p. 10–12

Laxmiprasad A. S., Raja V. S., Menon S., Goswami A., Rao M. V. H., Lohar K. A., 2013, Adv. Space Res., 52, 332

Li C. et al. 2015, Space Sci. Rev., 190, 85

Manju G., Pant, T.K., Sreelatha, P., Nalluveettil, S.J., Kumar, P.P., Upadhyay, N.K., Hossain, M.M., Naik, N., Yadav, V.K., John, R. and Sajeev, R., 2020. Lunar near surface plasma environment from Chandrayaan-2 Lander platform: RAMBHA-LP payload.,2020,CURRENT SCIENCE,118,383.

Meyer H. M., Denevi B. W., Robinson M. S., Boyd A. K., 2020, J. Geophys Res. Planets, 125

Mitrofanov I. G., Zelenyi L. M., Tret'yakov V. I., Kalashnikov D. V., 2021, Sol. Syst. Res., 55, 485
Ohtake M., Haruyama J., Matsunaga T., Yokota Y., Morota T., Honda C., Team L., 2008, Earth planet. space, 60, 257
Ouyang Z. et al. 2010, Science China Earth Sciences, 53, 1565
Paige D. A. et al. 2010, Space Sci. Rev., 150, 125
Pieters C. M. et al. 2009, Curr. Sci., 96, 500
Pieters C. M., Noble S. K., 2016, J. Geophys Res. Planets, 121, 1865
Shanmugam M. et al. 2020, Curr. Sci., 118, 53
Shyldkrot H., Shmidt E., Geron D., Kronenfeld J., Loucks M., Carrico J., Policastri L., Taylor J.. 2019, Proceedings of the AAS/AIAA Astrodynamics Specialist Conference, The first commercial lunar lander mission: Beresheet. p. 11
Sinha R. K. et al. 2020, Icarus, 337, 113449
Sinha R. K., Rani A., Ruj T., Bhardwaj A., 2023, Icarus, 402, 115636
Smith D. E. et al. 2010, Space Sci. Rev., 150, 209
Vasavada A. R., Paige D. A., Wood S. E., 1999, Icarus, 141, 179
Vondrak R., Keller J., Chin G., Garvin J., 2010, Space Sci. Rev., 150, 7
Wilhelms D. E., Howard K. A., Wilshire H. G., 1979. *Geologic Map of the South Side of the Moon*. Department of the Interior, US Geological Survey
Wu B., Li, F., Ye, L., Qiao, S., Huang, J., Wu, X. and Zhang, H., Topographic modeling and analysis of the landing site of Chang'E-3 on the Moon., 2014, Earth and Planetary Science Letters, 405, 257–273
Xiao L., Qian Y., Wang Q., Wang Q., 2021, Sample return missions, The Chang'e-5 mission. Elsevier, New York, p. 195
Zuber M. T. et al. 2013, Science, 339, 668
Zuo W., Li C., Zhang Z., 2014, Chin. J. Geochem., 33, 24

SUPPORTING INFORMATION

Supplementary data are available at *MNRASL* online.

Please note: Oxford University Press is not responsible for the content or functionality of any supporting materials supplied by the authors. Any queries (other than missing material) should be directed to the corresponding author for the article.

This paper has been typeset from a TEX/LATEX file prepared by the author.